

Direct Evidence for Diverse Source Complexity in Small Earthquakes (Mw3.3-5.0) Obtained from Short-Range Borehole Seismic Data

Keisuke Yoshida¹

¹Affiliation not available

December 10, 2023

Abstract

A good understanding of the rupture patterns of small earthquakes is essential to understand the differences between earthquakes of different sizes. However, resolving the source complexity of small events ($M_w < 5$) is challenging, because their seismic waveforms are distorted during propagation. In this study, we used high-quality seismic waveforms recorded by an excellent downhole sensor in Japan to directly examine the source complexities of 64 Mw3.3-5.0 short-range earthquakes (< 8 km). We found that even the waveforms of microearthquakes ($M_w < 2$) were simple at the sensor, indicating that the waveforms were scarcely disturbed by structural inhomogeneities. We inferred the moment rate functions from the shapes of the direct P-waves, which showed diversity in their complexity. Even conservatively estimated, 30% of the events had multiple subevents. The results suggest that methods that account for complexity, rather than those that assume a simple source pattern, are required to characterize even small earthquakes.

1 **Direct Evidence for Diverse Source Complexity in Small Earthquakes (Mw3.3-5.0)**

2 **Obtained from Short-Range Borehole Seismic Data**

3
4 Keisuke Yoshida

5
6 Research Center for Prediction of Earthquakes and Volcanic Eruptions, Graduate School
7 of Science, Tohoku University, Sendai, Japan

8
9 Corresponding author: Keisuke Yoshida, Research Center for Prediction of Earthquakes
10 and Volcanic Eruptions, Tohoku University, 6-6 Aza-Aoba, Aramaki, Aoba-Ku, Sendai,
11 980-8578, Japan (keisuke.yoshida.d7@tohoku.ac.jp)

12
13 **Key Points (<140 characters)**

- 14 1. Short-range (< 8 km) seismic waveforms at an excellent seismic sensor clearly show
15 the diversity in the complexity in 64 Mw3.3-5 events.
- 16 2. Even conservatively estimated, approximately 30% of the events had multiple pulses
17 that differed significantly from simple source models.
- 18 3. Methods that account for complexity rather than those that assume an a priori source
19 pattern are required to characterize small events.

20

21 **Abstract (150 ≤ 150 words)**

22 A good understanding of the rupture patterns of small earthquakes is essential to
23 understand the differences between earthquakes of different sizes. However, resolving the
24 source complexity of small events ($M_w < 5$) is challenging, because their seismic
25 waveforms are distorted during propagation. In this study, we used high-quality seismic
26 waveforms recorded by an excellent downhole sensor in Japan to directly examine the
27 source complexities of 64 $M_w 3.3-5.0$ short-range earthquakes (< 8 km). We found that
28 even the waveforms of microearthquakes ($M_w < 2$) were simple at the sensor, indicating
29 that the waveforms were scarcely disturbed by structural inhomogeneities. We inferred
30 the moment rate functions from the shapes of the direct P-waves, which showed diversity
31 in their complexity. Even conservatively estimated, 30% of the events had multiple
32 subevents. The results suggest that methods that account for complexity, rather than those
33 that assume a simple source pattern, are required to characterize even small earthquakes.

34

35 **Plain language summary (190 ≤ 200 words)**

36 It has been established that the source parameters of small earthquakes is similar to that
37 of large earthquakes. This suggests that small earthquakes ($M < 5$) may have a similar
38 degree of complexity as large earthquakes. However, the complexity of small earthquake
39 ruptures is usually masked by the propagation effect on seismic waveforms. In many cases,
40 the source parameters of small earthquakes are determined based on a model that assumes
41 that they are simple without any real complexity. To evaluate how often complex ruptures
42 of small earthquakes occur, high-quality seismic waveforms recorded by an excellent
43 downhole sensor in Japan for 64 $M_{3.3-5.0}$ short-range earthquakes (< 8 km) were used.
44 We confirmed that the waveforms recorded at this sensor are only slightly distorted by
45 propagation, directly showing the source process of the $M_{3.3-5.0}$ earthquakes. The shapes
46 of the direct P-waveforms show that their source processes are diverse and that more than
47 30 percent of the events have multiple subevents, unlike in commonly-used simple source
48 models. This suggests that the characterization of small earthquakes may require
49 quantities such as radiated seismic energy, which can be directly estimated even when
50 complex ruptures are considered.

51

52

53 **1. Introduction**

54 To fully understand earthquakes, information on the time history of the radiation
55 process is necessary. Moment-rate function (MRF) supplies essential information on
56 earthquake source processes. Many researchers have retrieved the MRFs of major
57 earthquakes ($M_w > 7$) and several MRF databases have been constructed for large
58 earthquakes, revealing the diversity of their ruptures (Tanioka & Ruff, 1997; Vallée et
59 al., 2011; Ye et al., 2016). However, for small earthquakes ($M_w < 5$), the retrieval of MRFs
60 is challenging because propagation effects strongly influence their waveforms.

61 Because of the difficulty in reliably estimating their details, the source parameters
62 for small earthquakes are often estimated using simple source process models. Precisely,
63 the stress drop of an earthquake is estimated based on the corner frequencies of the ω^2
64 source spectra of Aki (1967) and Brune (1970) with some pre-assumed source models.
65 Such models include those of Brune (1970), Sato and Hirasawa (1973), Madariaga (1978),
66 and Kaneko and Shearer (2014). The assumptions in the above approaches include that
67 earthquake rupture is characterized by a simple, single pulse. It is critical to verify the
68 validity of these assumptions.

69 Previous studies have established that earthquake rupture patterns are remarkably
70 similar for small and large earthquakes. Specifically, they reported that the stress drop
71 (e.g., Kanamori & Anderson, 1975) and moment-scaled radiated energy (e.g., Ide &
72 Beroza, 2001) are nearly constant, regardless of the static size of the earthquake. Still,
73 debate continues as to whether or not the moment-scaled radiated energy is scale
74 dependent (e.g., Abercrombie, 1995; Mayeda & Walter, 1996; Izutani & Kanamori, 2001;
75 Ide & Beroza, 2001; Pérez-Campos & Beroza, 2001; Prejean & Ellsworth, 2001; Takahashi
76 et al., 2005; Mayeda et al., 2005; Baltay et al., 2010; Malagnini et al., 2014; Nishitsuji &
77 Mori, 2014; Zollo et al., 2014; Denolle & Shearer, 2016; Ye et al., 2016; Chounet et al.,
78 2018). If the earthquake rupture is self-similar and independent of its static size, small
79 earthquakes may have a similar degree of complexity as large earthquakes. Based on the
80 empirical Green's function (EGF) approach (Mueller, 1985; Hough et al., 1997), several
81 recent studies have shown that the MRFs of small earthquakes have multiple pulses and a
82 certain complexity (Courboux et al., 1996; Kwiatek, 2008; Holmgren et al., 2019;

83 Pennington et al., 2023; Yoshida & Kanamori, 2023). Pennington et al. (2023) reported
84 that 60-80% of M_{2.6-3} events in the Pardfield area produced complex ruptures based on
85 the EGF approach. This EGF approach is almost the only method available for retrieving
86 the MRFs of small earthquakes (M_w<5). However, there is a risk of noise in the EGF, and
87 differences in reflected waves owing to slight differences in locations and focal
88 mechanisms can inadvertently make the MRFs appear more complex than they really are.

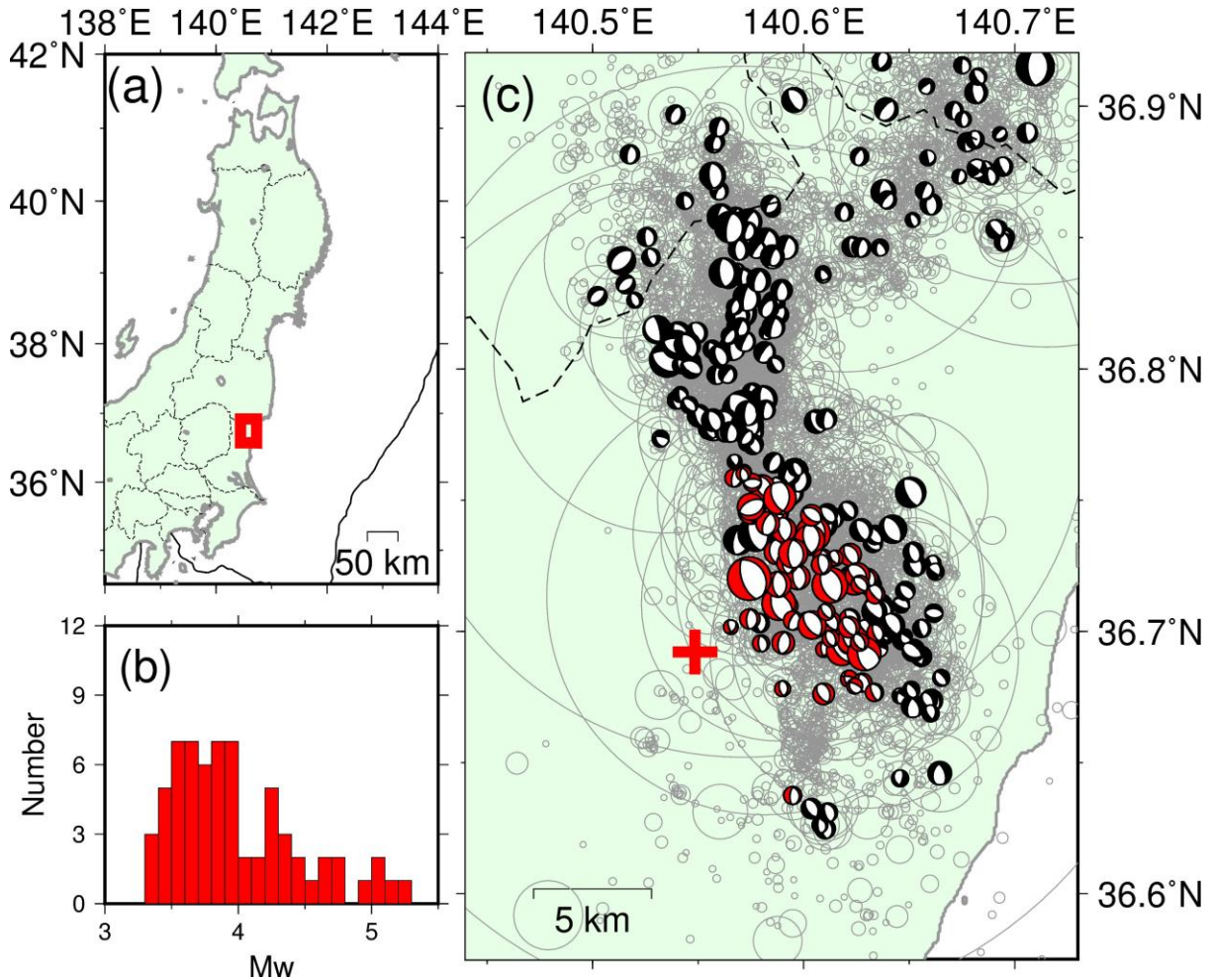
89 The most direct way to evaluate the complexities of MRFs is to directly examine
90 the displacement waveforms (Kikuchi & Ishida, 1988; Kanamori et al., 1990; Houston et
91 al., 1998; Harrington and Brodsky, 2009; Lin et al., 2016). This approach is simple but
92 unaffected by potentially problematic assumptions when dealing with EGFs, such as
93 negligible differences in path effects and focal mechanisms (Hutchings & Viegas, 2012),
94 noise in EGFs, and frequency-band limitations. Kanamori et al. (1990) showed that the
95 1988 Pasadena M_L4.9 event caused a two-pulse rupture based only on the waveforms at a
96 short-range single station (4 km). Kikuchi and Ishida (1988) used a similar approach to
97 examine the diversity in the shape of the MRFs of deep (z>50 km) earthquakes in Japan
98 from far-field P-waves. However, earthquake waveforms are typically affected by
99 propagation and site effects. The former effects (attenuation and scattering) become more
100 dominant with increasing source distances and frequencies. Because of their short rupture
101 durations and the need to investigate high frequencies, the MRFs of small earthquakes
102 (M_w<5) cannot be captured by observations at typical observation distances (> 20 km).
103 Additionally, soft near-surface sedimentary layers and heterogeneous velocity structures
104 strongly distort seismic waveforms. The use of a downhole sensor surrounded by hard
105 rocks with minimal amplification and attenuation is essential for retrieving source signals.
106 However, few situations exist in which these conditions are met.

107 In northern Ibaraki Prefecture, Japan, the National Research Institute for Earth
108 Science and Disaster Resilience (NIED) Hi-net operates an excellent borehole seismic
109 station (N.JUOH), which helps to investigate this issue. The downhole sensor of this
110 station is confined by granite rock with high velocity (V_p=5.4 km/s, V_s=3.2 km/s;
111 <https://www.kyoshin.bosai.go.jp/cgi-bin/kyoshin/db/siteimage.cgi?0+/IBRH14+kik+pdf>),
112 and the site amplification effect can be well taken into account. Intense seismicity has

113 occurred in this region since the 2011 M9 Tohoku earthquake (Fig. 1; more than 50,000
114 earthquakes of $M_{JMA} \geq 1$; Yoshida et al., 2015 and 2019), and this downhole sensor has
115 recorded many earthquake waveforms within ten kilometers.

116

117



118

119

120 **Figure 1.** (a) Map showing the location of the study region. The red rectangle indicates
121 the area shown in Fig. (c). (b) Histogram of M_w of the earthquakes to be analyzed. (c)
122 Map showing the study region. The red cross denotes the station (N. JUOH) whose
123 waveforms are analyzed in this study. The beach-balls represent the earthquake focal
124 mechanisms listed in the F-net moment tensor catalog (Kubo et al., 2002), with red ones
125 showing the events to be analyzed. Gray circles show the hypocenters of shallow
126 earthquakes ($z < 40$ km) with the JMA magnitude $M_{JMA} \geq 2.0$ from January 1, 2003, to
127 September 30, 2022. The circle sizes correspond to the diameters of Eshelby's (1957)

128 circular fault with a stress drop of 3 MPa.

129

130 This study examines the diversity of the MRFs of small earthquakes (M_w 3.3-5.0)
131 based on the close-range waveforms of direct P-waves. To evaluate the propagation effect,
132 which is a problem when looking directly at waveforms, we referred to the waveforms of
133 small earthquakes and synthetic waveforms based on a simple one-dimensional structure.
134 A comparison of the observed waveforms with their synthetic counterparts helps evaluate
135 the effects, including the geometrical spreading and surface reflections above the
136 downhole sensor.

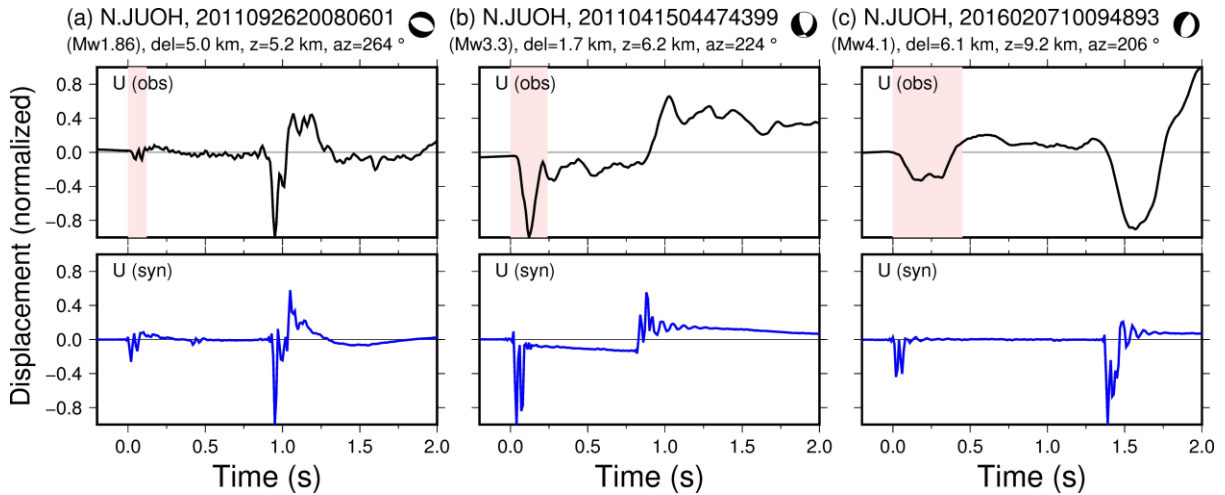
137

138 **2. Characteristics of Observed Waveforms**

139 Figure 2 shows the observed vertical components of the displacement waveforms
140 for three events. The seismometer was a 1 Hz velocity meter, and we removed the
141 instrument responses. The waveforms were very clean because of the short distances and
142 hard bedrock conditions. The first waveform is for the M_{JMA} 1.4 event, high-pass filtered
143 at 0.8 Hz to account for signal-to-noise ratio (Figs. 2a). The second and third correspond
144 to M_{JMA} 3.5 and M_{JMA} 4.4, respectively, high-pass filtered at 0.12 Hz (Figs. 2b-c). The
145 second waveform was recorded at a horizontal distance of 1.7 km from the hypocenter and
146 the contributions of intermediate and near-field terms between the onsets of P and S waves
147 (Fig. 2b). The P-waveform of the first event shows two pulses of approximately 0.04s
148 apart (pink area in Fig. 2a), which represent waves that arrived directly at the downhole
149 sensor and waves that arrived after being reflected by the ground surface directly above.

150

151



152

153 **Figure 2.** Displacement waveforms of three events obtained at the station to be used
 154 (N.JUOH) and the synthetic waveforms. Above: observed waveforms. Bottom: synthetic
 155 waveforms. The pink area indicates the direct P wave. The synthetic waveforms were
 156 estimated using the moment tensors estimated in this study, shown in this figure. The
 157 timing at which $t=0$ represents the onset of the P-wave.

158

159 The use of synthetic waveforms is helpful for evaluating the propagation effects.
 160 The code of Zhu and Rivera (2002), based on the wavenumber integration method, was
 161 used to compute synthetic waveforms. The assumed seismic wave velocity structure is
 162 Hasegawa et al. (1978), used in routine processing at Tohoku University. Based on the
 163 NIED Hi-net logging information, the velocities in the shallow 10 m was changed. The
 164 empirical relationship proposed by Brocher (2008) was used to assume depth-dependent
 165 density and Q structures (Fig. S1) following the procedure described by Yamaya et al.
 166 (2022). The source duration was set to 0.01s to obtain the impulse response. The moment
 167 tensors for $M_{JMA}3.5$ and $M_{JMA}4.4$ events were obtained from the F-net catalog (Kubo et
 168 al., 2002). The moment tensor solution for the $M_{JMA}1.4$ event was estimated by taking the
 169 amplitude ratios of nearby earthquakes listed in the nearby F-net moment catalog, based
 170 on the method of Yoshida et al. (2019).

171 The synthetic waveforms (vertical displacements) for these three events are shown
 172 in Fig. 2. These results agree well with the characteristics of the observed waveforms.
 173 The agreement for the $M_{JMA}1.4$ (Mw1.9) event at such high frequencies supports our
 174 assumption that these short-range data are scarcely disturbed by structural

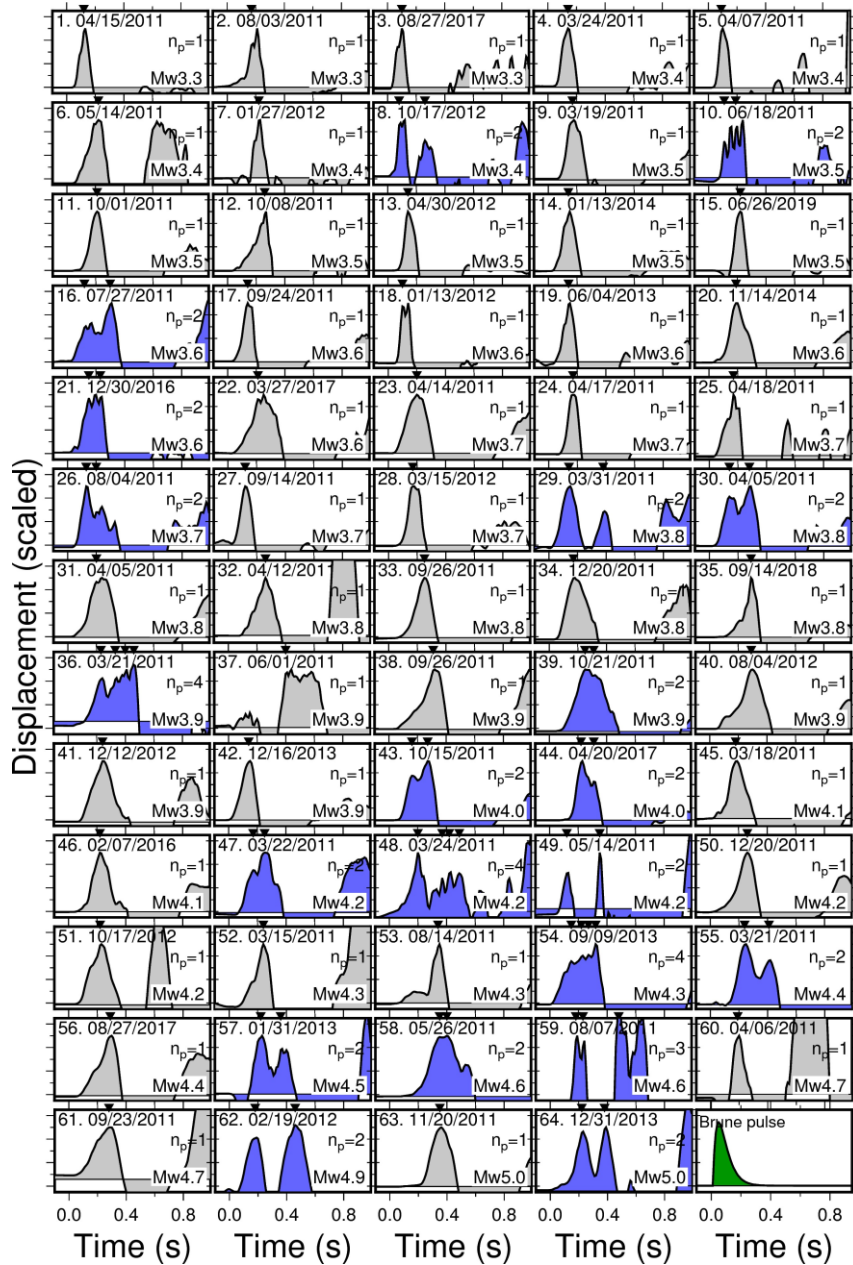
175 inhomogeneities. A comparison between the observed spectrum of the P wave of this event
176 and that of the synthetic one showed no systematic deviations (Fig. S2a). Although there
177 are slight deviations reflecting the incompleteness of the structural model, they are
178 negligible when discussing the macroscopic shape of the MRFs.

179 The details differ between the observed and synthetic waveforms for M_{JMA} 3.5 and
180 4.4 events because the synthetic waveforms do not include the effects of the MRFs (Figs.
181 2b-c). Reflecting this finiteness, the spectra of the observed waveforms of the two events
182 deviate from the synthetic spectra to smaller values above a certain frequency (corner
183 frequency) (Fig. S2b, c). This difference can be attributed to the effects of the MRFs on
184 these events.

185

186 **3. Complexity of moment-rate functions of 64 Mw3.3-5.0 events**

187 Figure 3 shows the P-wave displacement waveforms of the vertical component for
188 1.0 s for 64 target events. A high-pass filter (cutoff frequency of 0.5 Hz) was applied,
189 and the signs were adjusted to make the first onset positive. Waveforms for longer
190 windows (2.5 s) are shown in Fig. S3. The shapes of the direct P-waves show diversity;
191 some are simple, consisting of a single pulse (gray), whereas others are more complex
192 (blue).



193

194

195 **Figure 3.** Enlargement of direct P-waves for 64 M_w 3.3-5.0 earthquakes. They are
 196 arranged in order of M_w from smallest to largest. Triangles indicate the peaks of
 197 detected subevents. n_p indicates the number of detected subevents. The waveforms are
 198 shown in blue for earthquakes with more than two subevents. The lower right panel
 199 shows the MRF of Brune's (1970) model.

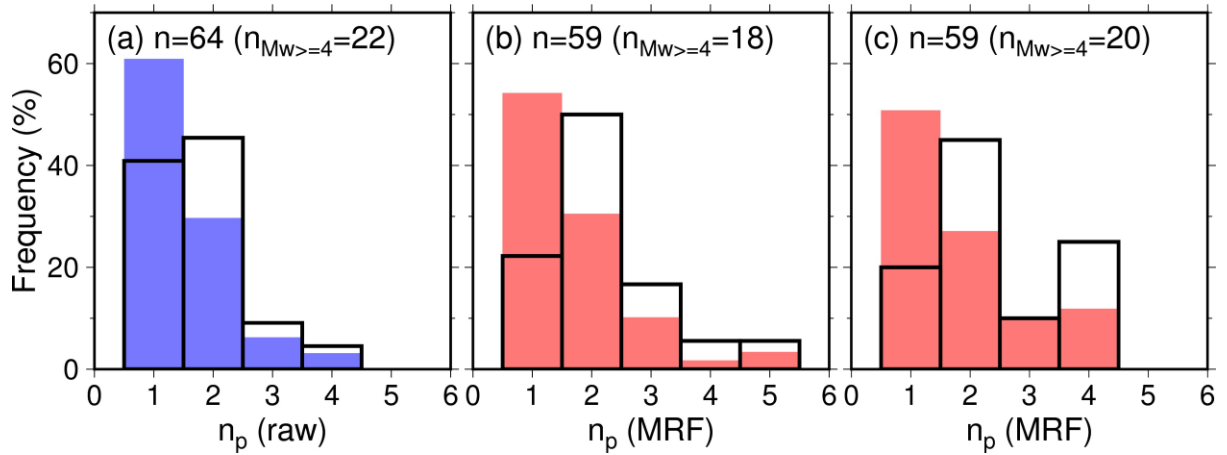
200

201 Given that the displacement waveform of the far-field P-wave is proportional to the
 202 MRF, this diversity may directly represent the diversity in the source process. In contrast,

203 the waveforms of the small earthquakes ($M_{JMA} < 2$) occurring in the vicinity (within 1 km)
204 of each earthquake were simple and similar, with essentially one pulse (Fig. S4). There
205 were exceptions with two short-interval pulses (< 0.04 s) due to surface reflections, as
206 shown in Fig. 2(a). This downhole sensor is located at a depth of 100 m. Therefore, two
207 pulses are naturally observed owing to surface reflection. The synthetic waveforms
208 computed at the location of each target event always had two pulses (Fig. S5). This effect
209 appears mainly at > 20 Hz and almost disappears when a 20 Hz low-pass filter is applied
210 (Fig. S6). Based on the empirical relationship of earthquakes in global settings by Duputel
211 et al. (2013), the centroid time of an $M_w 2$ event is approximately 0.028 s, which may
212 mask two pulses owing to surface reflection. The presence of surface reflections limits
213 the minimum duration of the MRFs inferred from direct inspection of the P-wave to
214 approximately 0.1 s.

215 The durations of the direct P-waves of the $M_w 3.3-5.0$ events are longer than 0.1 s
216 (Fig. 3). It is reasonable to assume that the diversity of the obtained P-waveforms of
217 $M_w 3.3-5.0$ events represents the diversity of the MRFs. Following Houston et al. (1998),
218 we measured the complexity using the number of subevents in the time function before
219 the S-wave arrival. The number of bumps was determined by the number of times the time
220 derivatives of the waveforms crossed zero. We imposed the following conditions to avoid
221 counting minor peaks due to surface reflections or noise: (1) The peak amplitude must be
222 greater than 50% of the amplitude of the maximum peak. (2) The time interval between
223 peaks should be greater than 0.05s. (3) The elapsed time from the previous peak should
224 be less than 0.5 s. Fig. 4(a) shows the histogram of the number of subevents thus obtained.
225 For 42 of the 64 events, the number of subevents was one, whereas for 22 events, the
226 number of subevents was two or more. Even when the observed waveforms of $M_w 3.3-5$
227 were low-pass filtered at 20 Hz, little change was observed in this trend (Fig. S7).

228
229
230
231



232

233

234 **Figure 4.** Histograms of the number of subevents estimated from the short-range
 235 waveforms and MRFs. The colored bars represent all events, and the lines indicate events
 236 with $M_w \geq 4.0$. (a) Direct P-wave, (b) MRFs obtained from the synthetic Green functions,
 237 and (c) MRFs obtained from the EGFs.

238

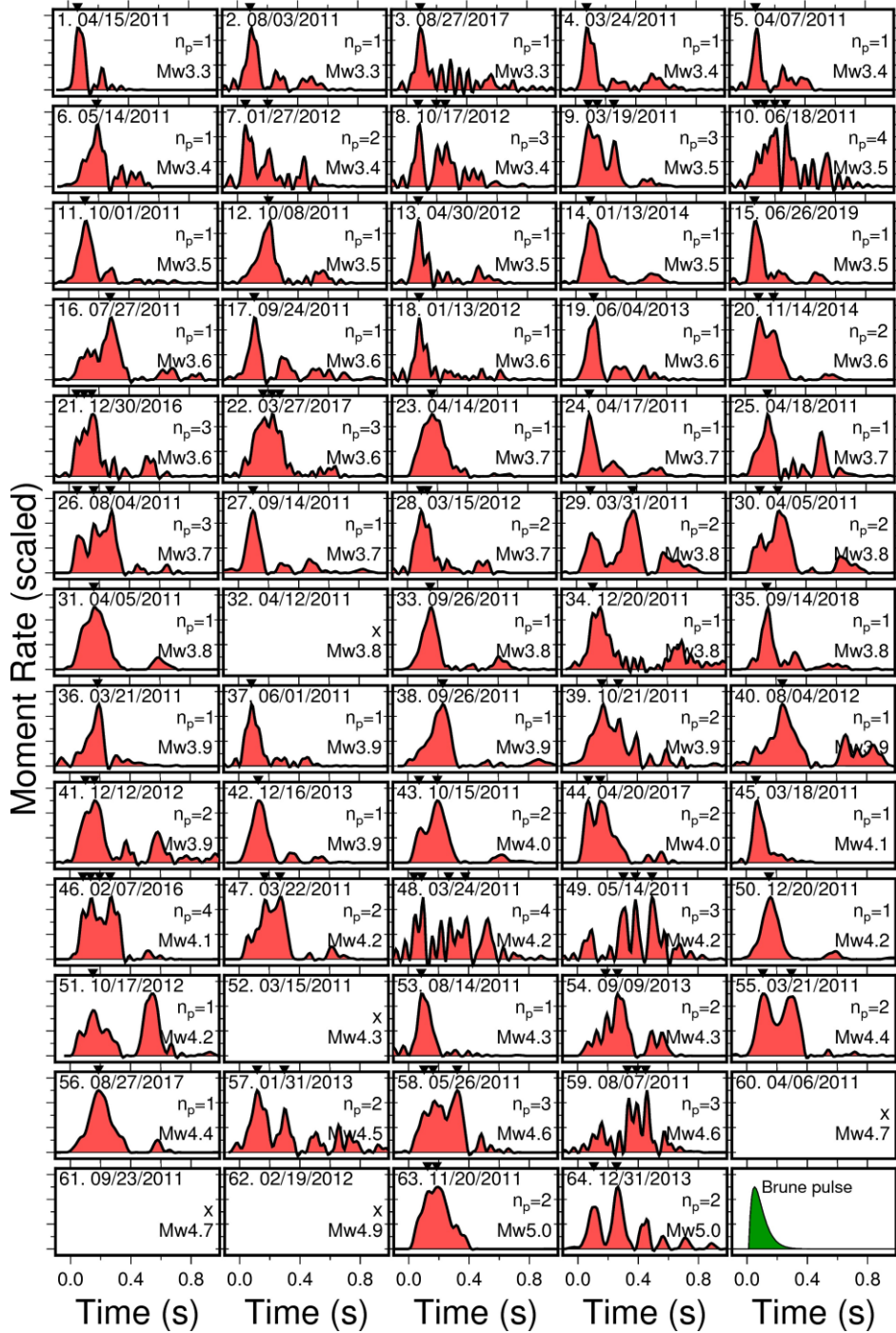
239 Our direct waveform inspection was slightly affected by propagation. To remove
 240 this contamination, we deconvolved the observed seismic waveforms using synthetic
 241 Green's functions (Fig. S6). These theoretical waveforms were computed based on the
 242 moment tensors and locations of each event. The hypocenter of each event was relocated
 243 based on the same velocity structure used to calculate the synthetic waveforms (Hasegawa
 244 et al., 1978), but from the hypocenters listed in the JMA catalog, with little change. For
 245 the deconvolution, we used the iterative time-domain deconvolution algorithm of Ligorria
 246 and Ammon (1999), which employs the method of Kikuchi and Kanamori (1982).
 247 Deconvolution was performed with a non-negative constraint using a 20 Hz Butterworth
 248 low-pass filter for stabilization, and results were obtained only when the recovery was
 249 greater than 80%.

250 Figure 5 shows the derived MRFs of 59 events. They maintained the original
 251 waveform shapes because of the minor impact of the propagation effect. Unlike the
 252 original waveforms, they were slightly affected by instability during deconvolution (e.g.,
 253 third or tenth event). However, counting the number of subevents from these MRFs, 27
 254 out of 59 events had two or more subevents (46%; Fig. 4b), similar to the original

255 waveform result. Similarly, Fig. 4(c) shows the number of subevents when deconvolution
256 was performed using the waveforms of nearby small earthquakes as the EGF (Figs. S8).
257 The frequency band was set to $f < 10$ Hz to avoid the effects of finite durations of small
258 events. This result is also similar to the original result, in that 29 of the 59 (49 %) had
259 multiple pulses. The increased proportion of complex events in the post-deconvolution
260 results may be due in part to the effects of the deconvolution instability.

261

262



263

264

265

266

267

268

269

270

Fig. 5. Estimated moment-rate functions based on the deconvolution by synthetic waveforms. Triangles indicate the peaks of detected subevents. n_p indicates the number of detected subevents. An x mark indicates an event for which deconvolution did not work. The lower right panel shows the MRF of Brune's (1970) model.

Compiling the results of previous studies that examined a few small events with an extensive network suggests that it is common for small events to exhibit complexity (Ide,

271 2001; Yamada et al., 2005; Uchide & Ide, 2010; Taira et al., 2015; Wu et al., 2019).
272 Yoshida and Kanamori (2023) studied more than 1700 Mw3-7 earthquakes in Japan based
273 on the radiated energy enhancement factor (REEF; Ye et al., 2018). Their results showed
274 that 30% of the analyzed events showed significant complexity (REEF>5), although the
275 used frequency range was relatively narrow (up to approximately 7 Hz for Mw4 events).
276 Those complex events tended to have significantly different source spectra from the ω^2 -
277 model, as expected (Madariaga, 1979). This study obtained consistent trends for 64
278 earthquakes by directly examining waveforms at a single station. Uchide and Imanishi
279 (2016) examined the source spectra of M3.2-4 events in this region by spectral ratios and
280 showed that many events deviate from the ω^2 -model. Combined with our time-domain
281 results, these may reflect a large number of complex events, even at this scale.

282 In the case of all three outcomes (Fig. 4), the number of subevents tends to be large
283 for events with $M_w \geq 4$, which may be at least partly attributed to the temporal resolution
284 of MRFs. With a given minimum resolvable duration (0.1 s) and sampling interval (0.01
285 s), resolving subevents for earthquakes with relatively short durations was difficult. This
286 suggests that our complexity estimate may be underestimated; when measured only for
287 Mw>4 earthquakes, 13 out of 22 events (59 %) showed multiple pulses.

288 Our estimated MRFs (Figs. 3, 4, and S8) exhibited various shapes. Some are simple
289 and have a single pulse, similar to the source models often used for the estimation of the
290 stress drop, such as those of Brune (1970), Sato and Hirasawa (1973), and Madariaga
291 (1978). The green MRF in Figs. 3 and 5 show the MRF of Brune (1970) for comparison.
292 However, even modest estimates show that approximately 30 % have multiple pulses that
293 differ significantly from the above source models. The widely used source models produce
294 erroneous results when applied to such complex events (Abercrombie, 2021; Liu et al.,
295 2023). The present results suggest that methods that account for complexity, rather than
296 those that assume a simple rupture pattern, are required to characterize even small
297 earthquakes. One approach is to estimate the spatial variation of a spatially heterogeneous
298 slip distribution/stress drop from seismic waveforms. However, the estimation
299 uncertainties are very large owing to the degrees of freedom (Adams et al., 2016).

300 The radiated energy is a different physical quantity than the stress drop, but can

301 be estimated in principle directly from seismic waveform data without requiring a specific
302 source model (e.g., Kanamori et al., 2020). Many source models have a one-to-one
303 relationship between the radiated energy and stress drop through model-specific radiation
304 efficiency. Ji et al. (2022) proposed estimating the stress drop based on radiated energy
305 because radiation efficiency takes similar values in various source models. Snoke (1987)
306 reported that estimating the stress drop from the apparent stress (moment-scale radiated
307 energy multiplied by rigidity) is more stable. However, because radiation efficiency is
308 not constant in reality (Venkataraman & Kanamori, 2004), it may be better to distinguish
309 between stress drop and (moment-scaled) radiated energy and directly use radiated energy.
310 Estimating the radiated energies of small earthquakes is not always straightforward
311 because of strong propagation effects and frequency band limitations (Abercrombie, 2021).
312 However, radiated energy is a quantity that can characterize small earthquakes regardless
313 of their complexity and may be a suitable parameter for characterizing the source process
314 of small earthquakes.

315

316 **4. Conclusion**

317 Short-range (< 8 km) seismic waveforms recorded at a downhole sensor surrounded
318 by granite ($V_p=5.4$ km/s, $V_s=3.2$ km/s) clearly show the diversity in the complexity of
319 the moment-rate functions for 64 M_w 3.3-5.0 earthquakes. Even conservatively estimated,
320 approximately 30% of the events had multiple pulses that differed significantly from
321 simple source models. These results suggest that methods that account for complexity,
322 rather than those that assume an a priori source process, are required to characterize even
323 small earthquakes. Despite the difficulties in estimation, the present results suggest that
324 using quantities such as radiated energy or moment-scale radiated energy is preferable as
325 they can be estimated without assuming an a priori source process.

326

327 **Acknowledgments**

328 I am grateful to Hiroo Kanamori for highlighting the importance of this short-range
329 observational data. We thank Toru Matsuzawa, Shunsuke Takemura, and Kentaro Emoto
330 for discussing waveform modeling, which helped improve the manuscript. The figures

331 were created using GMT (Wessel & Smith, 1998). This study was financially supported
332 by the JSPS KAKENHI (grant number JP 20K14569).

333

334 **Open Research**

335 Data Availability Statement

336 This study used hypocenter and arrival time data from the JMA-Unified Catalog
337 (<https://www.data.jma.go.jp/svd/eqev/data/bulletin/hypo.html>). Waveforms were
338 obtained from the NIED Hi-net website (<https://www.hinet.bosai.go.jp/?LANG=en>). They
339 were collected and stored by NIED Hi-net (2019). The figures were created using GMT
340 (Wessel and Smith, 1998).

341

342 **Reference**

343 Abercrombie, R. E. (1995). Earthquake source scaling relationships from -1 to 5 ML
344 using seismograms recorded at 2.5-km depth. *Journal of Geophysical Research*,
345 *100*(B12), 24015–24036. <https://doi.org/10.1029/95jb02397>

346 Abercrombie, R. E. (2021). Resolution and uncertainties in estimates of earthquake
347 stress drop and energy release. *Philosophical Transactions of the Royal Society A:*
348 *Mathematical, Physical and Engineering Sciences*, *379*(2196), 20200131.
349 <https://doi.org/10.1098/rsta.2020.0131>

350 Adams, M., Twardzik, C., & Ji, C. (2016). Exploring the uncertainty range of coseismic
351 stress drop estimations of large earthquakes using finite fault inversions.
352 *Geophysical Journal International*, *208*(1), 86–100.
353 <https://doi.org/10.1093/gji/ggw374>

354 Baltay, A., Prieto, G., & Beroza, G. C. (2010). Radiated seismic energy from coda
355 measurements and no scaling in apparent stress with seismic moment. *Journal of*
356 *Geophysical Research: Solid Earth (1978–2012)*, *115*(B8).
357 <https://doi.org/10.1029/2009jb006736>

358 Brocher, T. M. (2008). Key elements of regional seismic velocity models for long period
359 ground motion simulations. *Journal of Seismology*, *12*(2), 217–221.
360 <https://doi.org/10.1007/s10950-007-9061-3>

361 Brune, J. N. (1970). Tectonic stress and the spectra of seismic shear waves from
362 earthquakes. *J Geophys Res*, *75*(26), 4997–5009.
363 <https://doi.org/10.1029/jb075i026p04997>

364 Chounet, A., & Vallée, M. (2018). Global and Interregion Characterization of
365 Subduction Interface Earthquakes Derived From Source Time Functions Properties.

366 *Journal of Geophysical Research: Solid Earth*, 123(7), 5831–5852.
367 <https://doi.org/10.1029/2018jb015932>

368 Courboux, F., Virieux, J., Deschamps, A., Gibert, D., & Zollo, A. (1996). Source
369 investigation of a small event using empirical Green's functions and simulated
370 annealing. *Geophysical Journal International*, 125(3), 768–780.
371 <https://doi.org/10.1111/j.1365-246x.1996.tb06022.x>

372 Denolle, M. A., & Shearer, P. M. (2016). New perspectives on self-similarity for
373 shallow thrust earthquakes. *Journal of Geophysical Research: Solid Earth*, 121(9),
374 6533–6565. <https://doi.org/10.1002/2016jb013105>

375 Duputel, Z., Tsai, V. C., Rivera, L., & Kanamori, H. (2013). Using centroid time-delays
376 to characterize source durations and identify earthquakes with unique
377 characteristics. *Earth and Planetary Science Letters*, 374, 92–100.
378 <https://doi.org/10.1016/j.epsl.2013.05.024>

379 Eshelby, J. D. (1957). The determination of the elastic field of an ellipsoidal inclusion,
380 and related problems. *Proceedings of the Royal Society of London. Series A,*
381 *Mathematical and Physical Sciences*, 376–396.
382 <https://doi.org/10.1098/rspa.1983.0054>

383 Harrington, R. M., & Brodsky, E. E. (2009). Source Duration Scales with Magnitude
384 Differently for Earthquakes on the San Andreas Fault and on Secondary Faults in
385 Parkfield, California Source Duration Scales with Magnitude Differently on the San
386 Andreas Fault and on Secondary Faults. *Bulletin of the Seismological Society of*
387 *America*, 99(4), 2323–2334. <https://doi.org/10.1785/0120080216>

388 Hartzell, S. H. (1978). Earthquake aftershocks as Green's functions. *Geophysical*
389 *Research Letters*, 5(1), 1–4. <https://doi.org/10.1029/GL005i001p00001>

- 390 Hasegawa, A., Umino, N., & Takagi, A. (1978). Double-planed structure of the deep
391 seismic zone in the northeastern Japan arc. *Tectonophysics*, 47(1–2), 43–58.
392 [https://doi.org/10.1016/0040-1951\(78\)90150-6](https://doi.org/10.1016/0040-1951(78)90150-6)
- 393 Holmgren, J. M., Atkinson, G. M., & Ghofrani, H. (2019). Stress Drops and Directivity
394 of Induced Earthquakes in the Western Canada Sedimentary Basin Stress Drops and
395 Directivity of Induced Earthquakes in the Western Canada Sedimentary Basin.
396 *Bulletin of the Seismological Society of America*, 109(5), 1635–1652.
397 <https://doi.org/10.1785/0120190035>
- 398 Hough, S. E. (1997). Empirical Green’s function analysis: Taking the next step. *Journal*
399 *of Geophysical Research: Solid Earth*, 102(B3), 5369–5384.
400 <https://doi.org/10.1029/96jb03488>
- 401 Houston, H., Benz, H. M., & Vidale, J. E. (1998). Time functions of deep earthquakes
402 from broadband and short-period stacks. *Journal of Geophysical Research: Solid*
403 *Earth*, 103(B12), 29895–29913. <https://doi.org/10.1029/98jb02135>
- 404 Hutchings, L., & Viegas, G. (2012). Application of Empirical Green’s Functions in
405 Earthquake Source, Wave Propagation and Strong Ground Motion Studies.
406 *Earthquake Research and Analysis: New Frontiers in Seismology*.
- 407 Ide, S. (2001). Complex source processes and the interaction of moderate earthquakes
408 during the earthquake swarm in the Hida-Mountains, Japan, 1998. *Tectonophysics*,
409 334(1), 35–54. [https://doi.org/10.1016/S0040-1951\(01\)00027-0](https://doi.org/10.1016/S0040-1951(01)00027-0)
- 410 Ide, S., & Beroza, G. C. (2001). Does apparent stress vary with earthquake size?
411 *Geophysical Research Letters*, 28(17), 3349–3352.
412 <https://doi.org/10.1029/2001GL013106>

413 Ji, C., Archuleta, R. J., & Wang, Y. (2022). Variability of Spectral Estimates of Stress
414 Drop Reconciled by Radiated Energy. *Bulletin of the Seismological Society of*
415 *America*. <https://doi.org/10.1785/0120210321>

416 Kanamori, H., & Anderson, D. (1975). Theoretical basis of some empirical relations in
417 seismology. *Bulletin of the Seismological Society of America*, 65(5), 1073–1095.
418 Retrieved from <http://bssa.geoscienceworld.org/content/65/5/1073.short>

419 Kanamori, H., Mori, J., & Heaton, T. H. (1990). THE 3 DECEMBER 1988, PASADENA
420 EARTHQUAKE (ML = 4.9) RECORDED WITH THE VERY BROADBAND
421 SYSTEM IN PASADENA. *Bulletin of the Seismological Society of America*.

422 Kanamori, H., Ross, Z. E., & Rivera, L. (2020). Estimation of radiated energy using the
423 KiK-net downhole records - Old method for modern data. *Geophysical Journal*
424 *International*, 221(2), 1029–1042. <https://doi.org/10.1093/gji/ggaa040>

425 Kaneko, Y., & Shearer, P. M. (2014). Seismic source spectra and estimated stress drop
426 derived from cohesive-zone models of circular subshear rupture. *Geophysical*
427 *Journal International*, 197(2), 1002–1015. <https://doi.org/10.1093/gji/ggu030>

428 Kikuchi, M., & Ishida, M. (1993). Source retrieval for deep local earthquakes with
429 broadband records. *Bulletin of the Seismological Society of America*, 83(6), 1855–
430 1870. <https://doi.org/10.1785/bssa0830061855>

431 Kikuchi, M., & Kanamori, H. (1982). Inversion of complex body waves -. *Bulletin -*
432 *Seismological Society of America*, 72(2), 491–506.
433 <https://doi.org/10.1785/bssa0810062335>

434 Kubo, A., Fukuyama, E., Kawai, H., & Nonomura, K. (2002). NIED seismic moment
435 tensor catalogue for regional earthquakes around Japan: quality test and
436 application. *Tectonophysics*, 356(1–3), 23–48. [https://doi.org/10.1016/S0040-](https://doi.org/10.1016/S0040-1951(02)00375-X)
437 [1951\(02\)00375-X](https://doi.org/10.1016/S0040-1951(02)00375-X)

438 Kwiatek, G. (2008). Relative source time functions of seismic events at the Rudna
439 copper mine, Poland: estimation of inversion uncertainties. *Journal of Seismology*,
440 12(4), 499–517. <https://doi.org/10.1007/s10950-008-9100-8>

441 Ligorría, J. P., & Ammon, C. J. (1999). Iterative deconvolution and receiver-function
442 estimation. *Bulletin of the Seismological Society of America*, 89(5), 1395–1400.

443 Lin, Y.-Y., Ma, K.-F., Kanamori, H., Song, T.-R. A., Lapusta, N., & Tsai, V. C. (2016).
444 Evidence for non-self-similarity of microearthquakes recorded at a Taiwan borehole
445 seismometer array. *Geophysical Journal International*, 206(2), 757–773.
446 <https://doi.org/10.1093/gji/ggw172>

447 Liu, C., Lay, T., Wang, R., Taymaz, T., Xie, Z., Xiong, X., et al. (2023). Complex
448 multi-fault rupture and triggering during the 2023 earthquake doublet in
449 southeastern Türkiye. *Nature Communications*, 14(1), 5564.
450 <https://doi.org/10.1038/s41467-023-41404-5>

451 Malagnini, L., Mayeda, K., Nielsen, S., Yoo, S.-H., Munafo', I., Rawles, C., & Boschi,
452 E. (2014). Scaling Transition in Earthquake Sources: A Possible Link Between
453 Seismic and Laboratory Measurements. *Pure and Applied Geophysics*, 171(10),
454 2685–2707. <https://doi.org/10.1007/s00024-013-0749-8>

455 Mayeda, K., & Walter, W. R. (1996). Moment, energy, stress drop, and source spectra of
456 western United States earthquakes from regional coda envelopes. *Journal of*
457 *Geophysical Research B: Solid Earth*, 101(5), 11195–11208.
458 <https://doi.org/10.1029/96jb00112>

459 Mueller, C. S. (1985). Source pulse enhancement by deconvolution of an empirical
460 Green's function. *Geophysical Research Letters*, 12(1), 33–36.
461 <https://doi.org/10.1029/gl012i001p00033>

- 462 NIED. (2019). NIED Hi-net, National Research Institute for Earth Science and Disaster
463 Resilience. <https://doi.org/10.17598/NIED.0003>
- 464 Nishitsuji, Y., & Mori, J. (2014). Source parameters and radiation efficiency for
465 intermediate-depth earthquakes in Northeast Japan. *Geophysical Journal*
466 *International*, 196(2), 1247–1259. <https://doi.org/10.1093/gji/ggt458>
- 467 Pennington, C. N., Wu, Q., Chen, X., & Abercrombie, R. E. (2023). Quantifying rupture
468 characteristics of microearthquakes in the Parkfield Area using a high-resolution
469 borehole network. *Geophysical Journal International*, 233(3), 1772–1785.
470 <https://doi.org/10.1093/gji/ggad023>
- 471 Pérez-Campos, X., & Beroza, G. C. (2001). An apparent mechanism dependence of
472 radiated seismic energy. *Journal of Geophysical Research: Solid Earth*, 106(B6),
473 11127–11136. <https://doi.org/10.1029/2000jb900455>
- 474 Prejean, S. G., & Ellsworth, W. L. (2001). Observations of Earthquake Source
475 Parameters at 2 km Depth in the Long Valley Caldera, Eastern California. *Bulletin*
476 *of the Seismological Society of America*, 91(2), 165–177.
477 <https://doi.org/10.1785/0120000079>
- 478 Sato, T., & Hirasawa, T. (1973). Body wave spectra from propagating shear cracks.
479 *Journal of Physics of the Earth*. <https://doi.org/10.4294/jpe1952.21.415>
- 480 Snoke, J. A. (1987). STABLE DETERMINATION OF (BRUNE) STRESS DROPS.
481 *Bulletin of the Seismological Society of America*.
- 482 Taira, T., Dreger, D. S., & Nadeau, R. M. (2015). Rupture process for micro-
483 earthquakes inferred from borehole seismic recordings. *International Journal of*
484 *Earth Sciences*, 104(6), 1499–1510. <https://doi.org/10.1007/s00531-015-1217-8>
- 485 Takahashi, T., Sato, H., Ohtake, M., & Obara, K. (2005). Scale dependence of apparent
486 stress for earthquakes along the subducting pacific plate in northeastern Honshu,

487 Japan. *Bulletin of the Seismological Society of America*, 95(4), 1334–1345.
488 <https://doi.org/10.1785/0120040075>

489 Tanioka, Y., & Ruff, L. J. (1997). Source Time Functions. *Seismological Research*
490 *Letters*, 68(3), 386–400. <https://doi.org/10.1785/gssrl.68.3.386>

491 Uchide, T., & Ide, S. (2010). Scaling of earthquake rupture growth in the Parkfield area:
492 Self-similar growth and suppression by the finite seismogenic layer. *Journal of*
493 *Geophysical Research: Solid Earth (1978–2012)*, 115(B11).
494 <https://doi.org/10.1029/2009jb007122>

495 Vallée, M., J. Charléty, A. M. G. Ferreira, B. Delouis, J. Vergoz (2011). SCARDEC: a
496 new technique for the rapid determination of seismic moment magnitude, focal
497 mechanism and source time functions for large earthquakes using body - wave
498 deconvolution. *GEOPHYSICAL JOURNAL INTERNATIONAL*, 184, 338-358.
499 <https://doi.org/10.1111/j.1365-246X.2010.04836.x>

500 Venkataraman, A., & Kanamori, H. (2004). Observational constraints on the fracture
501 energy of subduction zone earthquakes. *Journal of Geophysical Research: Solid*
502 *Earth*, 109(5). <https://doi.org/10.1029/2003JB002549>

503 Wessel, P., & Smith, W. H. F. (1998). New, improved version of generic mapping tools
504 released. *Eos, Transactions American Geophysical Union*, 79(47), 579–579.
505 <https://doi.org/10.1029/98EO00426>

506 Wu, Q., Chen, X., & Abercrombie, R. E. (2019). Source Complexity of the 2015 Mw 4.0
507 Guthrie, Oklahoma Earthquake. *Geophysical Research Letters*, 46(9), 4674–4684.
508 <https://doi.org/10.1029/2019gl082690>

509 Yamada, T., Mori, J. J., Ide, S., Kawakata, H., Iio, Y., & Ogasawara, H. (2005).
510 Radiation efficiency and apparent stress of small earthquakes in a South African

511 gold mine. *Journal of Geophysical Research: Solid Earth* (1978–2012), 110(B1).
512 <https://doi.org/10.1029/2004jb003221>

513 Yamaya, L., Mochizuki, K., Akuhara, T., Takemura, S., Shinohara, M., & Yamada, T.
514 (2022). CMT inversion for small-to-moderate earthquakes applying to dense short-
515 period OBS array at off Ibaraki region. *Earth, Planets and Space*, 74(1), 164.
516 <https://doi.org/10.1186/s40623-022-01721-3>

517 Ye, L., Kanamori, H., & Lay, T. (2018). Global variations of large megathrust
518 earthquake rupture characteristics. *Science Advances*, 4(3), eaao4915.
519 <https://doi.org/10.1126/sciadv.aao4915>

520 Ye, L., Lay, T., Kanamori, H., & Rivera, L. (2016). Rupture characteristics of major and
521 great ($M_w \geq 7.0$) megathrust earthquakes from 1990 to 2015: 1. Source parameter
522 scaling relationships. *Journal of Geophysical Research: Solid Earth*.
523 <https://doi.org/10.1002/2015JB012426>

524 Yoshida, K., & Kanamori, H. (2023). Time-domain source parameter estimation of M_w
525 3–7 earthquakes in Japan from a large database of moment-rate functions.
526 *Geophysical Journal International*. <https://doi.org/10.1093/gji/ggad068>

527 Yoshida, K., Hasegawa, A., & Okada, T. (2015). Spatially heterogeneous stress field in
528 the source area of the 2011 M_w 6.6 Fukushima-Hamadori earthquake, NE Japan,
529 probably caused by static stress change. *Geophysical Journal International*, 201(2),
530 1062–1071. <https://doi.org/10.1093/gji/ggv068>

531 Yoshida, K., Saito, T., Emoto, K., Urata, Y., & Sato, D. (2019). Rupture directivity,
532 stress drop, and hypocenter migration of small earthquakes in the Yamagata-
533 Fukushima border swarm triggered by upward pore-pressure migration after the
534 2011 Tohoku-Oki earthquake. *Tectonophysics*, 769.
535 <https://doi.org/10.1016/j.tecto.2019.228184>

536 Yoshida, K., Hasegawa, A., Yoshida, T., & Matsuzawa, T. (2019). Heterogeneities in
537 Stress and Strength in Tohoku and Its Relationship with Earthquake Sequences
538 Triggered by the 2011 M9 Tohoku-Oki Earthquake. *Pure and Applied Geophysics*,
539 *176*(3), 1335–1355. <https://doi.org/10.1007/s00024-018-2073->

540

541